2013 IREP Symposium-Bulk Power System Dynamics and Control –IX (IREP), August 25-30, 2013, Rethymnon, Greece

A Production Simulation Tool for Systems with an Integrated Concentrated Solar Plant with Thermal Energy Storage

Ti Xu
University of Illinois at Urbana-Champaign

George Gross
University of Illinois at Urbana-Champaign

Abstract

The global awareness of the impacts of climate change is a key driver of the growing interest in effectively harnessing renewable energy resources. The *concentrated solar plant* (*CSP*) technology has emerged as a promising approach to harness solar energy, with several implementtations under way around the world. *CSP* is, typically, coupled with the deployment of thermal energy storage (*TES*) so as to provide the *CSP* operator the flexibility to produce electricity beyond the sunrise-to-sunset period. Indeed, the effective utilization of *TES* requires a scheduler to optimize the value of the *CSP*-produced energy. The assessment of *CSP* sets up an acute need for a practical simulation tool to study the effects of the integrated *CSP* with *TES* on the systems. Such a tool must explicitly represent the uncertainty, variability and intermittency of the solar resource and its interactions with the loads and other resources. We report on the development of a probabilistic simulation tool aimed at addressing these needs. The identification of distinct direct normal irradiation (*DNI*) patterns is an important step in the extension of the conventional probabilistic simulation approach to the systems with the integrated *CSP* resource. We use clustering techniques to identify the various pattern groups – referred to as regimes – and construct the *CSP* power output model based on the identified regimes. We make detailed use of conditional probability concepts in the incorporation of this model into the probabilistic production simulation approach. We carry out an extensive set of simulations for testing the extended approach. To illustrate the capabilities of this approach to quantify the variable effects of the systems with the integrated *CSP* resources over longer-term periods, we present the representative simulation results on a modified version of the *IEEE Reliability Test System* (*RTS*), with an integrated *CSP* resource. The load data is based from the scaled 2011 *ERCOT* load data. The study results provide insights into the *CSP* impacts on the variable effects of the systems and demonstrate the effectiveness of the extended simulation approach.

Introduction

Due to increasing awareness of the global climate change challenges, many countries are implementing renewable energy projects to generate cleaner energy. By 2010, renewable energy resources supplied about a sixth of the energy consumed throughout the world [1]. In the solar energy arena, *concentrated solar plant* (*CSP*) technology has recently experienced a steady growth, with 17 *GW* of *CSP* projects under development around the world [2]. Typically, *CSP* technology uses mirrors to reflect sunlight onto receivers and convert the collected solar energy into thermal energy, which is then used in a steam turbine or heat engine that drives a generator to produce electricity. Parabolic trough, solar tower, dish stirling, and linear Fresnel reflector, are the four common forms of *CSP* technologies. Compared to other *CSP* technologies, the primary difference of solar tower technology is the utilization of many large, flat mirrors, namely heliostats, to track the sun and focus the sunlight onto a central receiver [3]. A particularly beneficial feature of *CSP* is the incorporation of a thermal energy storage (*TES*) unit to store a fraction of the thermal energy for later use, possibly beyond the sunset [4]. As such, unlike photovoltaic or *PV* panels, a *CSP* resource can collect only the *DNI* and generate electricity beyond the time there is sunshine with the utilization of the *TES*. Still, the effective integration of *CSP* resources into the grid poses major challenges due to the inherent uncertainty, variability and intermittency nature of *DNI*. These characteristics impact markedly the times and the quantities of *CSP* energy production. Moreover, the efficient deployment of the *TES*, requires the use of a scheduler to optimize the contribution of the *CSP* resource to displace expensive and polluting conventional generation. Given the limited controllability of *DNI*, *CSP* resources can contribute whenever either solar or *TES* thermal energy is available. The extent to which the *CSP* energy production and the loads are correlated is, consequently, an important consideration in the evaluation of the *CSP* contribution. Unlike the difficult-to-predict variability of the *DNI*, the

978-1-4799-0199-9/13/$31.00

loads follow certain diurnal and weekly patterns, with higher demand during the weekdays than the weekends and with peaks, typically, at similar periods of the weekdays and lower values at nights. We illustrate in Fig.1 the shape of the hourly *DNI* at Midland, TX, in comparison with that of the *ERCOT* hourly load for a representative winter week. The plots clearly indicate the weakly correlated behavior of *DNI* with the loads [5], [6] which influences the impacts of the *CSP* contribution. The added flexibility afforded by the *TES* is a key reason for the growing interest in *CSP* [7]. The contribution of *CSP* resources is nearly 25 % of the *U.S.* utility-scale solar projects under development. By 2014, Spain will have installed 2.5 *GW CSP* resources, which will supply nearly 3 % of total electricity consumption in Spain [8]. Other countries involved in wide commercialization of *CSP* resources include China and Australia [9].

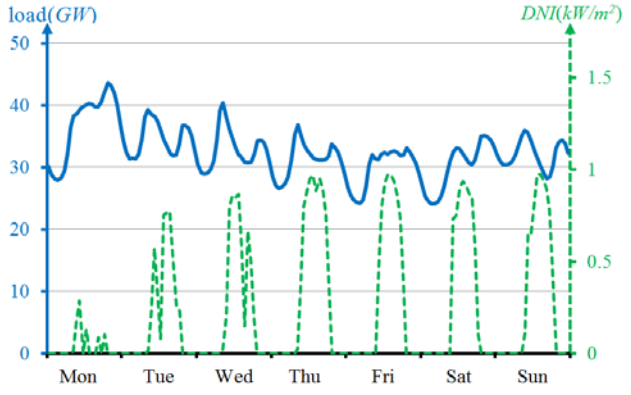

Fig.1: Plots of the chronological Midland, TX, DNI and the *ERCOT* hourly loads for the January 5–11, 2009 week

The increasing *CSP* role triggers an acute need for an appropriate simulation tool to effectively capture the nature of the *CSP* resources so as to quantify the variable effects of systems with integrated *CSP* resources. To evaluate these effects, such a tool needs to consider the operational schedule of the *CSP*, the time-varying and uncertain *DNI* patterns, and the interactions between *CSP* resources and loads and other resources. We address this need with the extension of the conventional probabilistic simulation to construct a practical simulation approach for systems with integrated *CSP* resources.

We construct the extended production simulation tool and simulate the systems with the integrated *CSP* resources with the explicit representation of the uncertainty in the *CSP* outputs, in addition to that of the controllable resources and loads. We use the extended approach to assess the impacts of systems with integrated *CSP* resources on the variable effects – the expected production costs, expected CO_2 emissions and reliability metrics. The extension of the simulation tool makes use of the regime-based *CSP* power output model we construct to represent the uncertainty in the *CSP* with *TES* outputs. We deploy statistical clustering techniques to obtain an analytic characterization of the *DNI* uncertainty using the historical hourly *DNI* for each season. We introduce a common time scale to allow the meaningful comparison of daily *DNI* patterns to find the clusters. We develop a systematic approach to derive the probabilistic *CSP* power output model, taking into account the *TES* schedule impacts, based on the regime characterization of *DNI* data to probabilistically represent the *CSP* power output for each regime. We incorporate the *CSP* power output model into probabilistic simulation framework by effective utilization of conditional probability concepts. In this way, the proposed methodology can explicitly represent the uncertainty and variability of the *CSP* outputs. The major application of the extended simulation tool is to quantify the variable effects of the systems with the integrated *CSP* resources over longer-term periods. We select some representative results from the extensive studies we performed to illustrate the application of the extended probabilistic simulation approach. The results are for a modified version of the *RTS* [10], with an integrated *CSP* resource, and use historical *DNI* and *ERCOT* load data. These results provide a good indication of the capabilities of the approach to effectively assess the variable effects in systems with integrated *CSP* resources.

The paper has four additional sections. In the second section, we focus on the *CSP* power output modeling and discuss in the third section the construction of the extended probabilistic simulation framework. In the fourth section, we present and discuss the representative results from various simulations performed. We summarize our contributions and provide directions for future work in the final section.

CSP Modeling

To quantify the longer-term impacts of the *CSP* resources integrated into the power systems, we construct a *CSP* power output model with the level of detail appropriate for representing the uncertainty, intermittency and variability nature of *DNI* and its impacts on the *CSP* output. We devote this section to the description of the probabilistic model, which we incorporate to construct our extended probabilistic simulation framework.

Since the daily *CSP* power output patterns depend on the daily *DNI* patterns, which vary significantly from one season to another, we build our model on a seasonal basis. We start our modeling with an explicit analysis on the seasonal *DNI* data set. We collect *DNI* data from historical observations for D days in a specific season.

We partition each day's sunrise-to-sunset period into M^d equal-duration sub-periods, with one observation from each sub-period. Let $a^{d,m}$ denote the *DNI* observed for the sub-period m of day d. We construct the vector $\underline{\boldsymbol{a}}^{(d)} = [a^{d,1}, a^{d,2}, \ldots, a^{d,M^d}]^T$ to collect the M^d *DNI* observations from day d. Since *DNI* is random, we can view $\underline{\boldsymbol{a}}^{(d)}$ as a realization of the *DNI* random variable (*r.v.*) vector $\underset{\sim}{\underline{A}}^{(d)} = [\underset{\sim}{A}^{d,1}, \underset{\sim}{A}^{d,2}, \ldots, \underset{\sim}{A}^{d,M^d}]^T$.

The fact that the duration of the sunrise-to-sunset period varies throughout the season and the year requires the introduction of a scaling scheme over the sunrise-to-sunset-period to allow the comparison of *DNI* patterns in a meaningful way [11]. The scaling scheme maps each realization $\underline{\boldsymbol{a}}^{(d)} \in \mathbb{R}^{M^d}$ into a common time scale with J equal sub-periods for each day d in a season. The transformation from the sunrise-to-sunset period for each day d requires a different scaling factor into J-subperiod scaled time frame to construct the vector $\underline{\boldsymbol{y}}^{(d)} = [y^{d,1}, y^{d,2}, \ldots, y^{d,J}]^T$, which collects the corresponding values of *DNI* for the J scaled sub-periods of day d. Here $y^{d,j}$ corresponds to the *DNI* for the scaled sub-period j of day d. In this way, we obtain the characterization $\underline{\boldsymbol{y}}^{(d)}$ to describe the *DNI* pattern of each day d in the scaled time frame. Conceptually, we view the time scaling process as the transformation of $\underline{\boldsymbol{a}}^{(d)}$ into $\underline{\boldsymbol{y}}^{(d)}$ as shown in Fig.2.

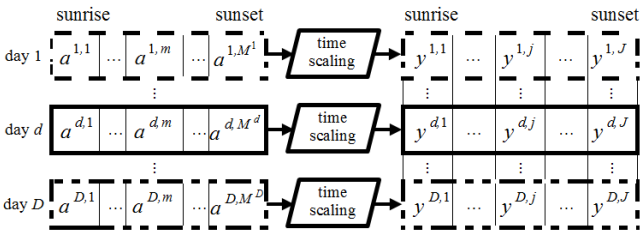

Fig.2: Diagram representation of scaling process for all days in data set

The collection $\mathcal{Y} = \{\underline{\boldsymbol{y}}^{(d)} : d = 1, 2, \ldots, D\}$ using the common time frame allows the identification of similar *DNI* patterns. In our paper, we deploy the *k-means clustering algorithm* to construct R different clusters [12], with each cluster grouping a subset of days with similar daily *DNI* patterns as shown in Fig.3. Conceptually, we view the cluster $\mathscr{R}_r$ to consist of realizations of the *r.v.*s $\underset{\sim}{Y}_r^j$ of the *DNI* for the scaled sub-periods $j = 1, 2, \ldots, J$. We can use the samples in the subset $\mathscr{R}_r$ to estimate the moments of each $\underset{\sim}{Y}_r^j$. In addition, the probability of each subset $\mathscr{R}_r$ is estimated by the ratio $\hat{\pi}_r = |\mathscr{R}_r| / D$, $r = 1, 2, \ldots, R$. In our work, we refer to the pair of $\hat{\pi}_r$ and the subset $\mathscr{R}_r$ as the regime denoted by $\mathcal{R}_r$.

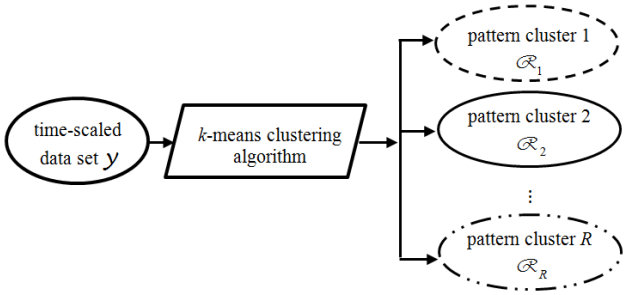

Fig.3: Diagram representation of clustering process

We deploy the regime-based time-scaled *DNI* patterns in the probabilistic simulation framework to sample from each cluster $\mathscr{R}_r$ to represent *DNI* patterns. However, such samples must be judiciously inverse-scaled and expressed in the time frame of the production simulation. For an arbitrary day d, the inverse-scaled representation covers the sunrise-to-sunset period, which consists of H^d equal-duration sub-periods. We assume that the *DNI* is constant in each inverse-scaled sub-period $h = 1, 2, \ldots, H^d$. Let $u^{d,h}$ be the *DNI* in the inverse-scaled sub-period h of day d and we construct $\underline{\boldsymbol{u}}^{(d)} = [u^{d,1}, u^{d,2}, \ldots, u^{d,H^d}]^T$, the *DNI* vector over H^d sub-periods of day d. We can view the inverse-scaling process as transformation of the common-time-scaled irradiation pattern into the inverse-scaled irradiation pattern over the sunrise-to-sunset period for day d. The regime-based *DNI* model allows us to use the samples in the subset $\mathscr{R}_r$ to compute the realizations of *r.v.* vector $\underset{\sim}{\underline{U}}_r^{(d)} = [\underset{\sim}{U}_r^{d,1}, \underset{\sim}{U}_r^{d,2}, \ldots, \underset{\sim}{U}_r^{d,H^d}]^T$, where $\underset{\sim}{U}_r^{d,h}$ represents *DNI r.v.* for the inverse-scaled sub-period h of day d conditioned on regime $\mathcal{R}_r$. We summarize the inverse-scaling process in Fig.4.

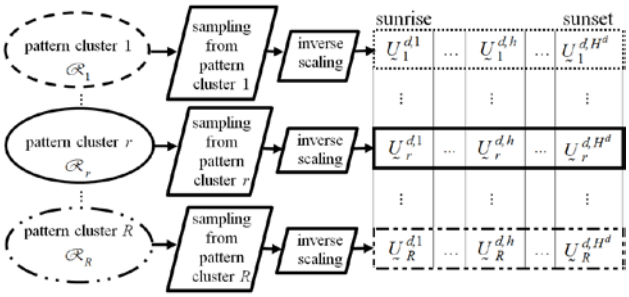

Fig.4: The inverse-scaled samples from the R clusters for the day d

We then discuss the steps to construct the probabilistic model of the *CSP* power output from the regime-based *DNI* model. For our purposes of this study, we start with focusing our analysis on the behavior of the *CSP*. The power output of the *CSP* depends on the nature of solar energy input, the specific details of the *CSP* configuration and the operational schedule. The appropriate utilization of thermal storage allows the *CSP* to produce electricity when solar energy is not available. For purposes of concreteness, we assume that the *TES* is operated so as to optimize the value of energy produced by the *CSP*. As the solar energy input is zero outside the sunrise-to-sunset period, the *CSP* power output must be zero before sunrise and may be nonzero after sunset under the appropriate employment of the *TES*. Thus we construct *CSP* power output vector $\underset{\sim}{\boldsymbol{p}}'^{(d)} = [p'^{d,1},\ p'^{d,2},\ \ldots,\ p'^{d,H'^d}]^T$, with $p'^{d,h}$, the *CSP* power output in the sub-period h of day d. The number of sub-periods H'^d covers the sunrise-to-midnight period for day d. Since the *DNI* is random, the *CSP* power output is also random. We may view $\underset{\sim}{\boldsymbol{p}}'^{(d)}$ as a realization of the *CSP* power output *r.v.* vector $\underset{\sim}{\boldsymbol{P}}'^{(d)} = [\underset{\sim}{P}'^{d,1},\ \underset{\sim}{P}'^{d,2},\ \ldots,\ \underset{\sim}{P}'^{d,H'^d}]^T$. Based on the analysis of the *CSP* behavior, we state the storage schedule optimization problem [13] as below with notations summarized in Appendix A:

$$\max_{\{\underset{\sim}{\boldsymbol{\kappa}}_\rho^{(d)},\underset{\sim}{\boldsymbol{\kappa}}_e^{(d)},\underset{\sim}{\boldsymbol{\kappa}}_c^{(d)},\ \underset{\sim}{\boldsymbol{\kappa}}_g^{(d)},\underset{\sim}{\boldsymbol{\zeta}}^{(d)},\underset{\sim}{\boldsymbol{p}}'^{(d)}\}} \sum_{h=1}^{H'^d} \bar{\gamma}^{d,h} \cdot p'^{d,h} \cdot \Delta \qquad (1a)$$

subject to

$$\left.\begin{aligned} \kappa_\rho^{d,h} &= \beta\,(u^{d,h}) \cdot \Delta \\ \kappa_\rho^{d,h} + \eta_g \kappa_g^{d,h} &= \kappa_c^{d,h} + \kappa_e^{d,h} \end{aligned}\right\} h = 1, 2, \ldots, H^d \qquad (1b)$$

$$\eta_g \kappa_g^{d,h} = \kappa_c^{d,h} + \kappa_e^{d,h} \qquad h = H^d, H^d+1, \ldots, H'^d \qquad (1c)$$

$$(1-\psi)(\zeta^{d,h} + \eta_c \kappa_c^{d,h} - \kappa_g^{d,h}) = \zeta^{d,h+1}$$
$$h = 1, 2, \ldots, H'^d - 1$$
$$(1-\psi)(\zeta^{d,h} + \eta_c \kappa_c^{d,h} - \kappa_g^{d,h}) \geq 0$$
$$h = H'^d \qquad (1d)$$

$$\left.\begin{aligned} p'^{d,h} &= \alpha(\kappa_e^{d,h} \Delta^{-1}) && (1e)\\ \zeta_{min} \leq \zeta^{d,h} &\leq \zeta_{max} && (1f)\\ \kappa_{c,min} \leq \kappa_c^{d,h} &\leq \kappa_{c,max} && (1g)\\ \kappa_{e,min} \leq \kappa_e^{d,h} &\leq \kappa_{e,max} && (1h)\\ \kappa_{g,min} \leq \kappa_g^{d,h} &\leq \kappa_{g,max} && (1i) \end{aligned}\right\} h = 1, 2, \ldots, H'^d$$

The objective function in $(1a)$ gives the value of the *CSP*-generated energy. The equality constraint in $(1b)$ represents the relationship between the absorbed thermal energy and the *DNI* for each sub-period from sunrise to sunset. The equality constraints in $(1c)$ represent the energy balance in the *CSP* for each sub-period during the sunrise-to-sunset period and during the sunset-to-midnight period, respectively. In $(1d)$, the two constraints state the thermal energy balance in the *TES*. The equality constraint in $(1e)$ represents the relationship between thermal energy into power block and the net electrical power output. The range of the variables is given in $(1f)-(1i)$ together with the limiting values of these ranges.

The solution of the storage schedule optimization problem is a realization of the *CSP* power output *r.v.* vector $\underset{\sim}{\boldsymbol{P}}'^{(d)}$, corresponding to $\underset{\sim}{\boldsymbol{U}}^{(d)}$. We can use inverse-scaled samples from each *DNI* pattern cluster $\mathcal{R}_r$ to compute the corresponding realizations of $\underset{\sim}{\boldsymbol{P}}'^{(d)}_r = [\underset{\sim}{P}'^{d,1}_r,\ \underset{\sim}{P}'^{d,2}_r,\ \ldots,\ \underset{\sim}{P}'^{d,H'^d}_r]^T$, the *CSP* power output *r.v.* vector conditioned on regime $\mathcal{R}_r$. We can assemble those realizations to construct the *CSP* power output sample space and use the values for sub-period h to estimate the *c.d.f.* and moments of $\underset{\sim}{P}'^{d,h}_r$.

To keep consistency with the midnight-to-midnight representation of the loads in the simulation approach, we construct the augmented *CSP* power output *r.v.* vector $\underset{\sim}{\boldsymbol{P}}^{(d)} \in \mathbb{R}^H$ for H sub-periods of day d in (2). Since there is no solar energy available before sunrise, we may view

each of the first $H - H'^{d}$ elements in $\underset{\sim}{\boldsymbol{P}}^{(d)}$ as an *r.v.* having value 0 associated with probability 1:

$$\begin{aligned}\underset{\sim}{\boldsymbol{P}}^{(d)} &= [\underset{\sim}{P}^{d,1},\ \underset{\sim}{P}^{d,2},\ \ldots,\ \underset{\sim}{P}^{d,H}]^T \\ &= [0,\ 0,\ \ldots,0,\underset{\sim}{P}'^{d,1},\ \underset{\sim}{P}'^{d,2},\ \ldots,\ \underset{\sim}{P}'^{d,H'^{d}}]^T \end{aligned} \quad (2)$$

The extended probabilistic simulation approach

The probabilistic simulation approach is widely deployed in the evaluation of the expected energy produced by each unit over a specified study period, the values of the reliability metrics, the expected system production costs, the expected greenhouse gas emissions and any other metric of interest to measure the variable effects. In this section, we briefly review the conventional probabilistic production simulation tool and describe the steps to extend the production simulation with an integrated *CSP* resource.

To emulate the operation of the power systems, we decompose the entire study period into W non-overlapping simulation periods and simulate probabilistically each period. We define and characterize each simulation period in a way that captures the seasonal characteristics and changes in the resource mix. Each simulation period has its own unit commitment set, resources characteristics and load characteristics. Let $\mathcal{T}_w = \{1, 2, \ldots, |\mathcal{T}_w|\}$ denote the index set of non-overlapping simulation sub-periods in the simulation period w. For each such sub-period, we assume that the load and each unit's output are constant.

For a unit to generate energy to serve the load, it must be first scheduled and thereafter be dispatched to supply the loads [14]. Let $\chi = \{1, 2, \ldots, |\chi|\}$ be unit index set of the controllable resource mix in our study and the subset $\chi^{(w)} \subset \chi$ be the committed unit index set for the simulation period w. Each block of a committed unit in $\chi^{(w)}$ is dispatched in the order of its marginal price and is used to meet the load in period w. In this way, we construct the period w loading order of committed units and we refer to this order as the loading list. Each controllable unit has its output level set by the plant operator, but the output is also a function of the availability of the unit. In our work, we model the availability of each controllable unit by a discrete outage capacity *r.v.*. We adopt a two-state probabilistic representation for each unit: either the full capacity is available or the unit is totally forced out. We also assume that each unit is independent of every other unit and of the load.

The probabilistic simulation approach makes use of the notion of equivalent load *r.v.*. We denote the load *r.v.* by $\underset{\sim}{L}$ and use equation (3) to compute the equivalent load *r.v.* iteratively:

$$\underset{\sim}{L}_k = \underset{\sim}{L}_{k-1} + \underset{\sim}{Z}_k \quad \text{with} \quad \underset{\sim}{L}_0 = \underset{\sim}{L} \quad (3)$$

In equation (3), $\underset{\sim}{L}_k$ represents the equivalent load *r.v.* needed to be served by the remaining units' blocks in the loading list after the first $k-1$ blocks are loaded and $\underset{\sim}{Z}_k$ represents the outage capacity *r.v.* of the k^{th} block to be loaded. Then we refer to the inverted load duration curve (*l.d.c.*) $\mathcal{L}_k$ as the complement of the *c.d.f.* of the equivalent load *r.v.* $\underset{\sim}{L}_k$. The independence assumption of load and units allows us to compute $\mathcal{L}_1, \mathcal{L}_2, \ldots, \mathcal{L}_k$ successively by convolution. We can make extensive use of the inverted *l.d.c.*s to evaluate the variable effects of the systems.

Then, the most important step to extend the production simulation approach to the systems with the integrated *CSP* resource is to mesh the probabilistic framework of production simulation with the probabilistic representation of the *CSP* output, which requires careful reexamination of the load representation. We describe this step using the hourly resolution with $|\mathcal{T}_w| = 168$ and $H = 24$, but the scheme is sufficiently general to allow the adoption of any desired granularity. In each simulation period w, we collect the daily load values for each day to obtain a subset of 24 hourly load values and construct the load *r.v.* sample space, which consists of $|\mathcal{T}_w|$ hourly load values. To directly relate the hourly *CSP* generation *r.v.* to the hourly load *r.v.*, we divide the load *r.v.* sample space into 24 subsets, with each subset containing realizations of the load *r.v.* $\underset{\sim}{L}|_h$ for each hour h. Consequently, we may view the sample space as a matrix with D_w rows and 24 columns. Let $\mathcal{T}_w^{(1)}, \mathcal{T}_w^{(2)}, \ldots, \mathcal{T}_w^{(24)}$ be the 24 subsets of $\mathcal{T}_w$, with each subset $\mathcal{T}_w^{(h)}$ being a collection of indices of the hour h for the D_w days in the simulation period w:

$$\mathcal{T}_w = \bigcup_{h=1}^{24} \mathcal{T}_w^{(h)} \tag{4}$$

$$\mathcal{T}_w^{(h_1)} \cap \mathcal{T}_w^{(h_2)} = \varnothing \qquad h_1 \neq h_2 \tag{5}$$

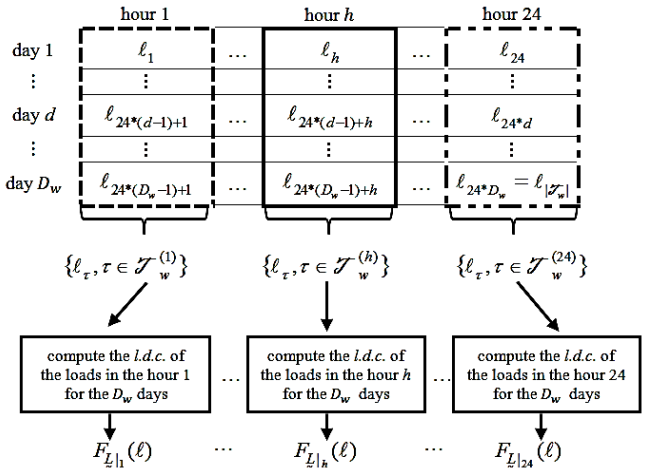

Fig.5: Process for the load classification

Fig.5 illustrates the process of the load classification. We make use of the load samples in each subset to estimate the *c.d.f.* $F_{\underset{\sim}{L}|_h}(\ell)$ of the load *r.v* conditioned on hour *h*. Since each of the 24 non-overlapping subsets has a uniform probability 1/24, the careful implementation of conditional probability allows us to restate the *c.d.f.* of $\underset{\sim}{L}$ as below:

$$\begin{aligned} F_{\underset{\sim}{L}}(\ell) &= Prob\{\underset{\sim}{L} \le \ell\} \\ &= Prob\{\underset{\sim}{L} \le \ell \ \text{in every hour}\} \\ &= \sum_{h=1}^{24} Prob\{\underset{\sim}{L}|_h \le \ell\} Prob\{\text{hour } h\} \\ &= \frac{1}{24} \sum_{h=1}^{24} Prob\{\underset{\sim}{L}|_h \le \ell\} \end{aligned} \tag{6}$$

Since the unit characteristics are uniform over the whole simulation period, i.e., for every hour, we can extend (6) to restate the *c.d.f.* of $\underset{\sim}{L}_k$ in the similar way:

$$F_{\underset{\sim}{L}_k}(\ell) = Prob\{\underset{\sim}{L}_k \le \ell\} = \frac{1}{24} \sum_{h=1}^{24} F_{\underset{\sim}{L}_k|_h}(\ell) \tag{7}$$

where the $F_{\underset{\sim}{L}_k|_h}(\ell)$ denotes the conditional probability of the equivalent load $\underset{\sim}{L}_k$ for hour *h*. In this way, we can restate all the probabilistic simulation results using the conditional distributions with the conditioning on the hour *h* of the simulation period.

We then describe the representation of the *CSP* resource impacts by making use of the load sample space partitioning in combination with the regime-based *CSP* power output. The uncertain *CSP* power output supplies the power systems with the remainder being served by the controllable resource mix. We refer to the remaining net load after the *CSP* is loaded as the "controllable load" $\underset{\sim}{C}$, which needs to be served by the controllable units. Assumption that the load and *CSP* power output *r.v.*s are independent for each hour allows us to compute the *c.d.f.* $F_{\underset{\sim}{C}_r|_h}(c)$ of the controllable load *r.v.* conditioned on each regime and each hour by convolution. In the similar way as the derivation of (6) and (7), we can restate the *c.d.f.* $F_{\underset{\sim}{C}_r}(c)$ of the controllable load *r.v.* conditioned on each regime:

$$\begin{aligned} F_{\underset{\sim}{C}_r}(c) &= Prob\{\underset{\sim}{C} \le c \mid \text{regime } \mathcal{R}_r\} \\ &= Prob\{\underset{\sim}{C} \le c \ \text{in every hour} \mid \text{regime } \mathcal{R}_r\} \\ &= \frac{1}{24} \sum_{h=1}^{24} F_{\underset{\sim}{C}_r|_h}(c) \end{aligned} \tag{8}$$

For each $F_{\underset{\sim}{C}_r}(\cdot)$, we perform the production simulation in the same way as in the conventional case but the computation is conditioned on each regime. In this way, we can evaluate the figures of merit of the controllable units conditioned on each regime $\mathcal{R}_r$. Subsequently, we can compute the expected value of each metric of interest as the probability weighted average of the expected values conditioned on the *DNI* regimes.

Simulation Study Results

We have completed the modification of conventional simulation framework to incorporate the regime-based *CSP* output model into the extended probabilistic production simulation tool. We illustrate the added capabilities of the tool by describing some representative results from the testing work we have done. We devote this section to discuss the test system used in the simulation results and to bring into evidence the capabilities of the extended simulation approach to

quantify the variable effects of the systems with an integrated *CSP* with *TES*. For these discussion purposes, we limit the results to a single year.

We discuss two sets of case studies carried out on a modified *RTS*. In case study set I, we investigate the impacts of deepening *CSP* capacities on the ststems. In the case set II, we carry out the studies on the systems with an integrated *CSP* for different *TES* capabilities. For the test system, the peak load is 3,050 *MW* and we use the appropriately scaled 2011 *ERCOT* load data, whose annual peak load is 67,859*MW* [5]. For each controllable unit in the *RTS* resource mix, we take the unit capacity, the outage capacity distribution and the economics of each of its blocks, with their respective capacities, into consideration. We represent the maintenance schedule for each unit in line with the requirements in the *RTS* specifications. We select the location of the *CSP* to be in Texas, specifically, at Midland – 32°21'N, 102°21'W. We use the historical *DNI* measurement data from the years 2003 to 2009 [6], [15] to identify the regimes for the simulation. We assume a solar tower structure for the *CSP* and the characteristics and deployment of heliostats and central receiver to be as specified for the system in the studies reported in [16] and [17]. In addition, we use the parameters of the *TES* and power block description in [18]. We use the Texas 2011 fuel costs and CO_2 emission rates [19]. For the *TES* schedule, we compute the objective function coefficients from past average hourly system marginal price data [5]. We summarize the two case study sets in Tables I and II, respectively.

Table I: Key characteristics of case study set I

study case	base case	c_{120}	c_{180}	c_{240}	c_{300}	c_{360}
CSP capacity (*MW*)	0	120	180	240	300	360
TES capability (*h*)	0	6				

Table II: Key characteristics of case study set II

study case	T_0	T_1	T_2	T_3	T_4	T_5	T_6
CSP capacity (*MW*)	120						
TES capability (*h*)	0	1	2	3	4	5	6

For simulation purposes, we group the 52 weeks of a year into four seasons so as to appropriately represent the seasonal characteristics. We identified from the available insolation data four *DNI* regimes $\mathcal{R}_r$, $r = 1, 2, \ldots, 4$, for each season. For the time scaling, we use $J = 80$ time-scaled sub-periods to characterize the daily *DNI* pattern. Table III shows the probability associated with each regime for each season. We display the centroid of each time-scaled daily *DNI* regime pattern for the summer season in Fig.6.

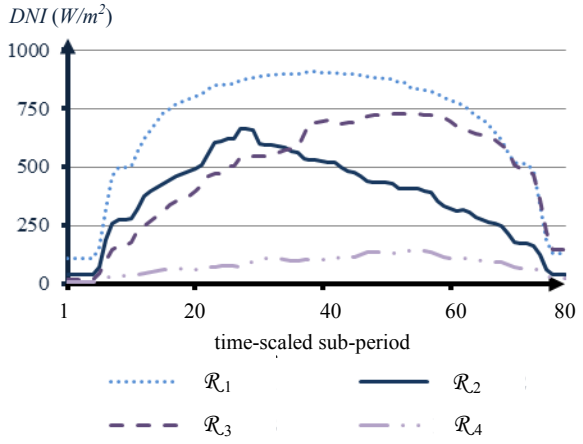

Fig.6: Centroid of each time-scaled daily *DNI* regime patterns for the summer

Table III: The probability of each *DNI* regime at Midland, TX in years from 2003 to 2009

regime	season			
	S_1	S_2	S_3	S_4
$\mathcal{R}_1$	0.450	0.413	0.483	0.418
$\mathcal{R}_2$	0.231	0.250	0.220	0.253
$\mathcal{R}_3$	0.165	0.185	0.154	0.176
$\mathcal{R}_4$	0.154	0.152	0.143	0.154

We start out the discussion of case study set I with the base case for the supply system consisting only of the controllable resources. We present in Table IV the values of the reliability – the loss of load probability (*LOLP*) and the expected unserved energy (*EUE*), the expected production costs and CO_2 emissions metrics for a representative winter and summer weeks and for the entire year.

Table IV: Simulation results for base case without the *CSP*

metric	simulation period		
	week of Jan. 10–16, 2011	week of Jul. 25–31, 2011	entire 2011
LOLP	$1.68\ 10^{-6}$	$3.40\ 10^{-3}$	$1.90\ 10^{-3}$
EUE (*MWh*)	$2.01\ 10^{-2}$	71.15	2,520
expected production costs (*million $*)	5.15	11.3	357
expected CO_2 emissions (*million ton*)	0.16	0.30	10.31

Next, we present in Table V the simulation results on the test system with an integrated 120 *MW CSP* ($\mathcal{C}_{120}$). The implementation of the solar plant reduces the *LOLP* and *EUE* indices by 32.83 and 35.05 %, respectively, reflecting the reliability improvement in the system due to the *CSP* integration with respect to the base case results. Similarly, the *CSP* integration lowers the expected production costs and CO_2 emissions by 4.22 and 3.17 %, respectively. We display in Figs.7 and 8 the simulation results in case study set I in terms of the changes in each metric with respect to the base case. We note that the expected production costs and the expected CO_2 emissions decrease essentially linearly as the *CSP* capacity increases. Such results are reasonable since every additional *MW* of *CSP* generation displaces the energy of more costly and polluting units. The CO_2 emissions of each unit are assumed to be linearly dependent on the unit production and so the lowered CO_2 emissions behave accordingly. We also observe the diminishing returns in reliability improvement. Although the integration of *CSP* with higher power capacity lowers the *LOLP* and the *EUE*, the reliability improvement of each successive increment has lower impact than the preceding increment.

Table V: Simulation results for Case $\mathcal{C}_{120}$ with a 120 *MW* solar tower

metric	simulation period		
	week of Jan. 10-16, 2011	week of Jul. 25–31, 2011	entire 2011
LOLP	$1.60\ 10^{-6}$	$2.12\ 10^{-3}$	$1.30\ 10^{-3}$
EUE(MWh)	$1.92\ 10^{-2}$	41.80	$1.64\ 10^{-3}$
expected production costs (*million $*)	5.05	10.8	342
expected CO_2 emissions (*million ton*)	0.161	0.29	9.98

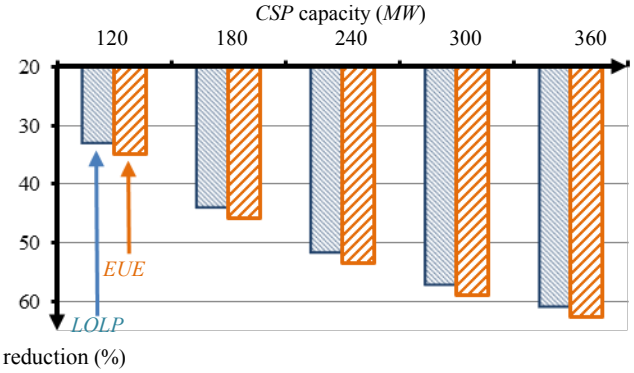

Fig.7: The reductions in *LOLP* and *EUE* indices vis-à-vis the base case values for the capacity sensitivity in case set I

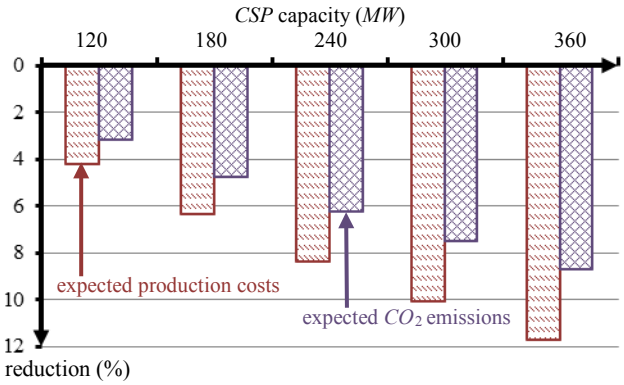

Fig.8: The reductions in the expected cost and CO_2 emission indices vis-à-vis the base case values for the capacity sensitivity in case set I

We can see how well the extended simulation framework captures the seasonal characteristics from the simulation results of Case $\mathcal{C}_{240}$. Table VI displays the simulation results for the summer conditioned on each identified regime together with the weighted average. The production simulation results differ markedly in distinct regimes of the summer period. For instance, the *LOLP* conditioned on regime $\mathcal{R}_4$ is over twice larger than that conditioned on regime $\mathcal{R}_2$. This is because those daily *DNI* patterns in regime $\mathcal{R}_2$ represent the *DNI* pattern with higher solar energy. Thus, the simulation results clearly illustrate the strong dependence of reliability and economic impacts on the various daily *DNI* patterns.

Table VI: Seasonal simulation results for summer in Case $\mathcal{C}_{240}$

metric	regime				S_2
	$\mathcal{R}_1$	$\mathcal{R}_2$	$\mathcal{R}_3$	$\mathcal{R}_4$	
LOLP (10^{-4})	23.01	31.44	28.97	61.95	33.35
EUE (10^2 *MWh*)	7.00	10.95	8.79	19.99	10.66
production costs (10^8 *$*)	1.18	1.26	1.23	1.36	1.24
expected CO_2 emissions (*million ton*)	3.09	3.27	3.19	3.49	3.22

In Table VII, we display the simulation results for four seasons and the entire 2011 year. Since summer has relatively high energy demand, the *LOLP* of S_2 is almost 200 times of that of S_3 and the expected CO_2 emissions of S_4 is less than 50 % of that of S_2. Hence, the simulation results explicitly demonstrate the strong correlation between reliability and economic impacts of the integrated *CSP* resource and the seasonal characteristics of the system.

Table VII: Seasonal simulation results for the entire year in Case C_{240}

metric	season				entire 2011 year
	S_1	S_2	S_3	S_4	
LOLP (10^{-4})	3.61	33.35	0.17	0.11	9.38
EUE (10^2 *MWh*)	0.94	10.66	0.035	0.021	11.70
production costs (10^8 *$*)	0.83	1.24	0.60	0.60	3.27
expected CO_2 emissions (*million ton*)	2.47	3.22	1.96	2.01	9.66

We present in Figs.9 and 10 the simulation results in case study set II in terms of the changes in each metric with respect to the base case. We can notice that the expected value of each metric decreases with the increasing *TES* capability since more thermal energy can be stored during the daytime for later use. We also observe the diminishing returns in the improvement of each metric. Particularly, when the *TES* capability becomes more than 3 *hour*, the change of each metric is trivial. This is because the solar energy of each day is not sufficient enough for the *CSP* to make full use of a *TES* with larger capability.

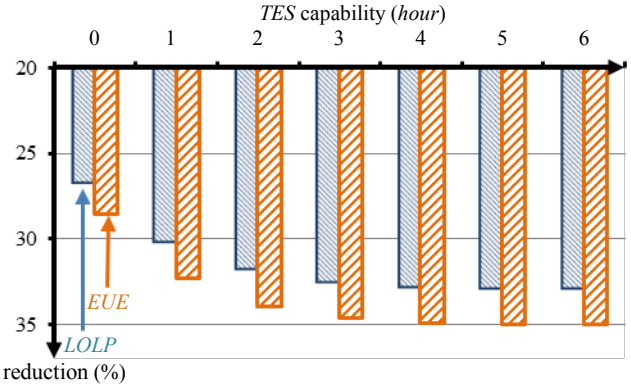

Fig.9: The reductions in *LOLP* and *EUE* indices vis-à-vis the base case values for the capacity sensitivity in case set II

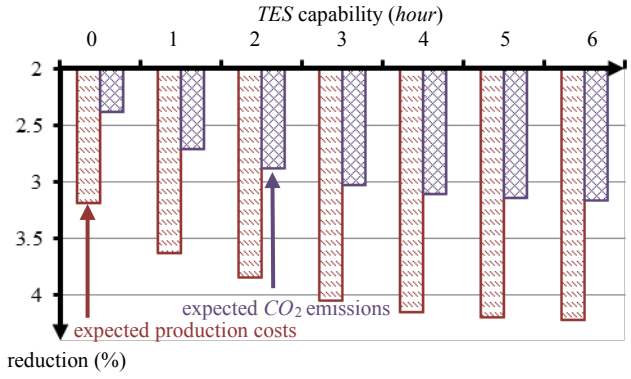

Fig.10: The reductions in the expected cost and CO_2 emission indices vis-à-vis the base case values for the capacity sensitivity in case set II

Those key metrics and the representative simulation results presented in this section provide strong evidence to prove that the extended simulation approach is effectively capable to capture the time-varying characteristics of the *CSP* resource and quantify its impacts on the systems.

Conclusion

In this paper, we present the development of an extended simulation approach to assess the variable effect impacts of power systems with integrated *CSP* resources over longer-term periods. The ability to quantify the impacts of *CSP* resources on the economics of electricity supply, the emission outputs and the system reliability results in an effective methodology for planning, investment decision, regulatory filing, and policy analysis applications. The representative results discussed illustrate the ability of the approach to answer a wide array of *what if* questions on *CSP* integration for realistic power systems. Our results are selected from the extensive studies we carried out to quantify the impacts of *CSP* resource integration on the system variable effects for a wide variety of parametric studies. Our work provides valuable insights into the role that *CSP* resources can play in the effective harnessing of solar energy and the efficient deployment of *TES* in the integration of such resources. The extended simulation approach, incorporating the representation of integrated *CSP* resources, constitutes a significant improvement in the capability to emulate systems with integrated uncertain, time-varying, and intermittent solar resources with *TES*.

The proposed approach is a good basis to develop a comprehensive simulation framework to investigate the variable effects of systems with the integrated *CSP* and wind resources at multiple sites. In addition, we will explore the representation of parabolic trough technology and assess the influence of the integrated *CSP* resources on the systems with location diversity. The advantages of the regime-based characterization of *DNI* to capture both the seasonal and diurnal variability of variable energy resources can be exploited in other areas. We will report on such efforts in future publications.

References

[1] J. L. Sawin et al., "renewable energy 2012 global status report," 2013, REN21, Paris, France. [Online]. Available: http://www.map.ren21.net/GSR/ GSR2012.pdf.

[2] U. Wang, "the rise of concentrating solar thermal power," 2011, *Renewable Energy World.* . [Online].Available: http://www.renewableenergyworld.com/rea/news/article/2011/06/the-rise-of-concentrating-solar-thermal-power

[3] M. Mendelsohn et al., "Utility-Scale Concentrating Solar Power and Photovoltaics Projects: A Technology and Market Overview," NREL, Golden, CO, 2009.

[4] IRENA, "Concentrating solar power," *Renewable energy technologies: cost analysis series*, vol.1, no.2, Jun.2012.
[5] ERCOT, "Hourly load data archives," 2012, Elctric Reliability Council of Texas, Austin, TX. Available: http://www.ercot.com/ gridinfo/load/load_hist/
[6] NREL, "National solar radiation database - 1991-2010 update," 2012, National Renewable Energy Laboratory, Golden, CO. [Online].Available:http://rredc.nrel.gov/solar/old data/nsrdb/1991-2010/hourly/list by state.html
[7] U. Herrmann et al., "Two-tank molten salt storage for parabolic trough solar power plants," *Energy*, vol.29, no. 5-6, pp. 883–893, 2004
[8] K. Elliott, "Spain's CSP market: Get set for a technology race,"2011, CSP today, London, UK. [Online]. Available: http://social.csptoday.com/techn ology/spains-csp-market-get-set-technology-race
[9] S. H. Madaeni et al., "How Thermal Energy Storage Enhances the Economic Viability of Concentrating Solar Power," *Proceedings of the IEEE* , vol.100, no.2, pp. 335-347, Feb. 2012
[10] C. Grigg et al., "The IEEE reliability test system-1996. A report prepared by the reliability test system task force of the application of probability methods subcommittee,"," *IEEE Trans. Power Syst*., vol. 14, no.3, pp. 1010–1020, Aug. 1999
[11] R. Bhana, "A production simulation tool for systems with integrated photovoltaic energy resources," M.S. thesis, Dept. Elect. & Comp. Eng., Univ. of Ilinois, Urbana-Champaign, IL, 2011
[12] R. Xu and D. C. Wunsch, "partitional clustering", in *Clustering,* John Wiley & Sons Inc., Hoboken, New Jersey, pp. 67-72, 2009.
[13] R. Dominguez, et al., "Optimal offering strategy for a concentrating solar power plant," *Applied Energy*, vol. 98, pp.316-325, 2012
[14] G. Gross, "Electricity Resource Planning", class notes for ECE 588, Dept. Elect. & Comp. Eng., Univ. Ilinois, Urbana-Champaign, Fall 2012.
[15] NOAA, "*Climate Data for Stations,*" National Oceanic and Atmospheric Admistration, Silver Spring, MD. [Online]. Available: http://www7.ncdc.noaa.gov/CDO/dataproduct
[16] M. Wagner, "Simulation and Predictive Performance Modeling of Utility-Scale Central Receiver System Power Plants," Dept. Mech. Eng., Univ. Wisconsin, Madison, 2006
[17] NREL, "Solar Advisor Model," 2012, National Renewable Energy Laboratory, Golden, CO. [Online]. Available: https://sam.nrel.gov/
[18] A. M. Patnode, "Simulation and Performance Evaluation of Parabolic Trough Solar Power Plants." Dept. Mech. Eng., Univ. Wisconsin, Madison, 2006
[19] EIA, "Monthly Energy Review," 2011, Energy Information Administration, Washington D.C. [Online]. Available: http://www.eia.gov/totalenergy/data/ monthly/ index.cfm

Appendix A: Nomenclature

D number of days for *DNI* data collection

M^d number of non-overlapping sub-periods over the sunrise-to-sunset period of day d

$a^{d,m}$ *DNI* observed for the sub-period m of day d

$\underline{\boldsymbol{a}}^{(d)}$ *DNI* vector $[a^{d,1}, a^{d,2}, \ldots, a^{d,M^d}]^T$ for M^d sub-periods over the sunrise-to-sunset period of day d

$\underset{\sim}{\underline{\boldsymbol{A}}}^{(d)}$ *DNI r.v.* vector $[\underset{\sim}{A}^{d,1}, \underset{\sim}{A}^{d,2}, \ldots, \underset{\sim}{A}^{d,M^d}]^T$ for M^d sub-periods over the sunrise-to-sunset period of day d

J number of time-scaled sub-periods over the sunrise-to-sunset period

$y^{d,j}$ *DNI* observed for the time-scaled sub-period j of day d

$\underline{\boldsymbol{y}}^{(d)}$ *DNI* vector $[y^{d,1}, y^{d,2}, \ldots, y^{d,J}]^T$ for J time-scaled sub-periods over the sunrise-to-sunset period of day d

$\mathscr{R}_r$ *DNI* pattern cluster r, where $r = 1, 2 \ldots\ldots R$

$\hat{\pi}_r$ estimated probability of $\mathscr{R}_r$

$\mathcal{R}_r$ *DNI* pattern regime, where $r = 1, 2 \ldots\ldots R$

$\underset{\sim}{Y}_r^j$ *DNI r.v.* for the time-scaled sub-period j of day d conditioned on regime $\mathcal{R}_r$

H^d number of non-overlapping inverse-scaled sub-periods over the sunrise-to-sunset period of day d

$u^{d,h}$ *DNI* observed for the inverse-scaled sub-period h of day d

$\underline{\boldsymbol{u}}^{(d)}$ *DNI* vector $[u^{d,1}, u^{d,2}, \ldots, u^{d,H^d}]^T$ for H^d inverse-scaled sub-periods over the sunrise-to-sunset period of day d

$\underset{\sim}{U}_r^{d,h}$ *DNI r.v.* conditioned on $\mathcal{R}_r$ for the inverse-scaled sub-period h of day d

$\underset{\sim}{\underline{\boldsymbol{U}}}_r^{(d)}$ *DNI r.v.* vector $[\underset{\sim}{U}^{d,1}, \underset{\sim}{U}^{d,2}, \ldots, \underset{\sim}{U}^{d,H^d}]^T$ for H^d inverse-scaled sub-periods over the sunrise-to-sunset period of day d

H'^d number of non-overlapping sub-periods over the sunrise-to-midnight period

$p'^{d,h}$ *CSP* power output in the sub-period h of day d

$\underline{\boldsymbol{p}}'^{(d)}$ *CSP* power output vector $[p'^{d,1}, p'^{d,2}, \ldots, p'^{d,H'^d}]^T$ for H'^d sub-periods over the sunrise-to-midnight period of day d

Δ duration of one sub-period in the *TES* schedule optimization problem

$\kappa_\rho^{d,h}$ absorbed thermal energy by the *CSP* in the sub-period h of day d

$\underline{\boldsymbol{\kappa}}_{\rho}^{(d)}$ absorbed thermal energy vector $[\kappa_{\rho}^{d,1}, \kappa_{\rho}^{d,2}, \ldots, \kappa_{\rho}^{d,H^d}]^T$ for H^d sub-periods over the sunrise-to-sunrise period of day d

$\beta(\cdot)$ nonlinear mapping of *DNI* into absorbed thermal energy flow rate

$\overline{\gamma}^{d,h}$ objective function coefficient from past average hourly system marginal price data for the sub-period h of day d

$\kappa_c^{d,h}$ thermal energy charged into the *TES* in the sub-period h of day d

$\underline{\boldsymbol{\kappa}}_c^{(d)}$ charging thermal energy vector $[\kappa_c^{d,1}, \kappa_c^{d,2}, \ldots, \kappa_c^{d,H'^d}]^T$ for H'^d sub-periods over the sunrise-to-midnight period of day d

η_c charging efficiency of *TES*

$\kappa_g^{d,h}$ thermal energy discharged from *TES* in the sub-period h of day d

$\underline{\boldsymbol{\kappa}}_g^{(d)}$ discharging thermal energy vector $[\kappa_g^{d,1}, \kappa_g^{d,2}, \ldots, \kappa_g^{d,H'^d}]^T$ for H'^d sub-periods over the sunrise-to-midnight period of day d

η_g discharging efficiency of *TES*

$\kappa_e^{d,h}$ total thermal energy delivered from the solar field and *TES* into the power block of *CSP* in the sub-period h of day d

$\underline{\boldsymbol{\kappa}}_e^{(d)}$ vector representation $[\kappa_e^{d,1}, \kappa_e^{d,2}, \ldots, \kappa_e^{d,H'^d}]^T$ of thermal energy into the power block for H'^d sub-periods over the sunrise-to-midnight period of day d

ψ thermal energy loss rate in the *TES*

$\zeta^{d,h}$ thermal energy stored in *TES* in the sub-period h of day d

$\zeta^{(d)}$ thermal energy stored in *TES* vector $[\zeta^{d,1}, \zeta^{d,2}, \ldots, \zeta^{d,H'^d}]^T$ for H'^d sub-periods over the sunrise-to-midnight period of day d

$\kappa_{\rho,max}, \kappa_{\rho,min}$ limit values of $\kappa_{\rho}^{d,h}$

$\kappa_{g,max}, \kappa_{g,min}$ limit values of $\kappa_g^{d,h}$

$\kappa_{e,max}, \kappa_{e,min}$ limit values of $\kappa_e^{d,h}$

ζ_{max} thermal storage capacity of the *CSP*

ζ_{min} minimum thermal energy stored in the *TES*

$\alpha(\cdot)$ nonlinear mapping of thermal energy flow rate into net electrical power output

$\underset{\sim}{P}'^{d,h}$ *CSP* power output *r.v.* in the sub-period h of day d

$\underline{\underset{\sim}{\boldsymbol{P}}}'^{(d)}$ *CSP* power output *r.v.* vector $[\underset{\sim}{P}^{d,1}, \underset{\sim}{P}^{d,2}, \ldots, \underset{\sim}{P}^{d,H'^d}]^T$ for H'^d sub-periods over the sunrise-to-midnight period of day d

$\underset{\sim}{P}'^{d,h}_r$ *CSP* power output *r.v.* for the sub-period h of day d conditioned on regime $\mathcal{R}_r$

$\underline{\underset{\sim}{\boldsymbol{P}}}'^{(d)}_r$ *CSP* power output *r.v.* vector $[\underset{\sim}{P}^{d,1}|_r, \underset{\sim}{P}^{d,2}|_r, \ldots, \underset{\sim}{P}^{d,H'^d}|_r]^T$ for H'^d sub-periods over the sunrise-to-midnight period of day d conditioned on regime $\mathcal{R}_r$

$\underline{\underset{\sim}{\boldsymbol{P}}}^{(d)}$ augmented *CSP* power output *r.v.* vector $[\underset{\sim}{P}^{d,1}, \underset{\sim}{P}^{d,2}, \ldots, \underset{\sim}{P}^{d,H}]^T$ over the midnight-to-midnight period of day d

W number of simulation periods in the whole study period

w simulation period

D_w number of days in the simulation period w

$\mathcal{T}_w$ sub-period index set of simulation period w

$\mathcal{T}_w^{(h)}$ subset of $\mathcal{T}_w$, containing the indices of the hour h of the D_w days in simulation period w

$\underset{\sim}{L}_k$ equivalent load *r.v.* after the first $k-1$ blocks in loading priority list are loaded

$\underset{\sim}{L}_k|_h$ equivalent load *r.v.* conditioned on hour h after the first $k-1$ blocks in loading priority list are loaded

$F_{\underset{\sim}{L}_k}(\ell)$ *c.d.f.* of the equivalent load *r.v.* $\underset{\sim}{L}_k$

$F_{\underset{\sim}{L}_k|_h}(\ell)$ *c.d.f.* of the hourly equivalent load *r.v.* $\underset{\sim}{L}_k|_h$

$\underset{\sim}{Z}_k$ outage capacity *r.v.* of the k^{th} block

$\underset{\sim}{C}$ controllable load *r.v.*

$\underset{\sim}{C}_r$ controllable load *r.v.* conditioned on regime $\mathcal{R}_r$

$F_{\underset{\sim}{C}_r}(\cdot)$ *c.d.f.* of the controllable load *r.v.* $\underset{\sim}{C}_r$